Original Article

High angular resolution diffusion imaging (HARDI) of porcine menisci: a comparison of diffusion tensor imaging and generalized q-sampling imaging

Qi Zhao[1,2], Abigail Holt[3], Charles E. Spritzer[2], Louis E. DeFrate[3,4], Amy L. McNulty[3,4,5], Nian Wang[6,7,8]

[1]Physical Education Institute, Jimei University, Xiamen, China; [2]Department of Radiology, Duke University School of Medicine, Durham, NC, USA; [3]Department of Orthopaedic Surgery, Duke University School of Medicine, Durham, NC, USA; [4]Department of Biomedical Engineering, Duke University, Durham, NC, USA; [5]Department of Pathology, Duke University School of Medicine, Durham, NC, USA; [6]Department of Radiology and Imaging Sciences, Indiana University, Indianapolis, IN, USA; [7]Stark Neurosciences Research Institute, Indiana University, Indianapolis, IN, USA; [8]Indiana Center for Musculoskeletal Health, Indiana University, Indianapolis, IN, USA

Contributions: (I) Conception and design: N Wang, Q Zhao; (II) Administrative support: N Wang, Q Zhao; (III) Provision of study materials or patients: A Holt, LE DeFrate, AL McNulty; (IV) Collection and assembly of data: Q Zhao, A Holt, N Wang; (V) Data analysis and interpretation: Q Zhao, CE Spritzer, LE DeFrate, AL McNulty, N Wang; (VI) Manuscript writing: All authors; (VII) Final approval of manuscript: All authors.

Correspondence to: Nian Wang, PhD. Department of Radiology and Imaging Sciences, Indiana University, GH, Suite 4102, 355 West 16th Street, Indianapolis, IN 46202, USA; Stark Neurosciences Research Institute, Indiana University, Indianapolis, IN, USA; Indiana Center for Musculoskeletal Health, Indiana University, Indianapolis, IN, USA. Email: nianwang@iu.edu.

Background: Diffusion magnetic resonance imaging (MRI) allows for the quantification of water diffusion properties in soft tissues. The goal of this study was to characterize the 3D collagen fiber network in the porcine meniscus using high angular resolution diffusion imaging (HARDI) acquisition with both diffusion tensor imaging (DTI) and generalized q-sampling imaging (GQI).

Methods: Porcine menisci (n=7) were scanned *ex vivo* using a three-dimensional (3D) HARDI spin-echo pulse sequence with an isotropic resolution of 500 µm at 7.0 Tesla. Both DTI and GQI reconstruction techniques were used to quantify the collagen fiber alignment and visualize the complex collagen network of the meniscus. The MRI findings were validated with conventional histology.

Results: DTI and GQI exhibited distinct fiber orientation maps in the meniscus using the same HARDI acquisition. We found that crossing fibers were only resolved with GQI, demonstrating the advantage of GQI over DTI to visualize the complex collagen fiber orientation in the meniscus. Furthermore, the MRI findings were consistent with conventional histology.

Conclusions: HARDI acquisition with GQI reconstruction more accurately resolves the complex 3D collagen architecture of the meniscus compared to DTI reconstruction. In the future, these technologies have the potential to nondestructively assess both normal and abnormal meniscal structure.

Keywords: Diffusion tensor imaging (DTI); generalized q-sampling imaging (GQI), tractography; meniscus; high angular resolution diffusion imaging (HARDI)

Submitted Sep 22, 2023. Accepted for publication Feb 19, 2024. Published online Mar 20, 2024.
doi: 10.21037/qims-23-1355
View this article at: https://dx.doi.org/10.21037/qims-23-1355

Introduction

The crescent-shaped menisci are important connective tissues positioned between the tibia and femur in the knee joint. While the menisci help provide stability to the knee, the main function of these tissues is to transmit and distribute forces during joint movement (1,2). The inner zone of the tissue contains both type I and type II collagen and proteoglycans, while the outer zone is predominantly composed of type I collagen (1). Within this inhomogeneous structure, there are interdigitated circumferential and radial collagen fibers that provide strength and resistance to tensile forces as the joint is loaded (2). Disruption of the complex 3D architecture alters the ability of the meniscus to transmit loads through the joint, and ultimately is a risk factor for the development of osteoarthritis (OA) (3). Thus, a methodology to quantify disruptions to the 3D fiber network of the meniscus would be an important advance in understanding the early structural changes that contribute to OA development.

Magnetic resonance imaging (MRI) is the primary imaging modality used for evaluating meniscus integrity (4-7). Multiple pulse sequences have been developed to detect meniscal tears, including gradient recalled acquisitions, proton density weighted spin echo sequences, fast spin echo proton density sequences, and T2 weighted sequences (8). However, a limitation of most conventional MRI techniques in clinical use is the short T2 relaxation times of many tissues within the knee, including the menisci (9-12). Quantitative MRI (qMRI) techniques, including T2 mapping, T1ρ mapping, and delayed Gadolinium Enhanced MRI of Cartilage (dGEMRIC) have been investigated as tools to assess the biochemical alterations in the meniscus before morphological changes occur (13-18). More recently, Ultrashort echo-time T2* (UTE-T2*) mapping has been proposed as a novel quantitative technique with the potential to measure short-T2* relaxation times for joint tissues that are not well captured with standard T2 mapping (19,20). Although these measurements provide valuable quantitative parameters related to meniscus biochemical properties, directly identifying collagen fiber orientation and alignment remains challenging using these relaxation time-based techniques.

Diffusion MRI (dMRI) allows for the quantification of water diffusion properties and the assessment of directional anisotropy in soft tissues (21,22). Recently, diffusion tensor imaging (DTI) and tractography have been performed to visualize the 3D collagen fiber network of the meniscus (23). However, a significant limitation of DTI is that only a single fiber orientation can be calculated within each imaging voxel (21,24). High angular resolution diffusion imaging (HARDI) with generalized q-sampling imaging (GQI) reconstruction is a dMRI technique that has been used in tissues such as brain and cartilage with the capability of resolving crossing fibers at the voxel level (25,26).

As there is currently limited work quantifying the collagen fiber structure in the meniscus using dMRI (25), the goal of this study was to characterize the 3D collagen fiber network in the porcine meniscus using HARDI acquisition with both DTI and GQI reconstruction methods. Since GQI has been used to resolve crossing fibers in other tissues (27), we hypothesized that GQI reconstruction will resolve the radial and circumferential fibers in the meniscus, providing a more accurate representation of the structure of the meniscus compared to DTI.

Methods

Specimen preparation

Seven porcine menisci were harvested from the knee joints of skeletally-mature female pigs obtained from a local abattoir. The menisci were fixed in 10% formalin (VWR, Radnor, PA, USA) for 3 days at 4 ℃. Then the menisci were immersed in a phosphate-buffered saline (PBS) solution containing 0.5% Prohance (Bracco Diagnostics Inc., Princeton, NJ, USA) to shorten T1 relaxation times to about 105 ms, allowing for a reduction in scan time.

Microscopic MRI (μMRI) protocols

The menisci were scanned at 7.0 Tesla in a small animal MRI system (Magnex Scientific, Yarnton, Oxford, UK) equipped with 650 mT/m gradient coils (Resonance Research Inc., MA, USA) (*Figure 1*). The orientation of each sample was kept consistent within the magnet in order to minimize magic angle effects. A 3D HARDI spin-echo pulse sequence was performed for all scans. Radio frequency (RF) transmission and reception were achieved using a custom-made coil. The acquisition parameters were as follows: matrix size =96×60×40, FOV =48×30×20 mm^3, 500 μm isotropic spatial resolution, echo time (TE) =10.8 ms, repetition time (TR) =100 ms, b value of 1,000 s/mm^2. In order to explore the effects of the b value on tractography, measurements were performed at b values of 100 and 1,000 s/mm^2. Specifically, the same 61 diffusion gradient encoding directions and 6 non-diffusion-weighted (b0) measurements were performed for each b value.

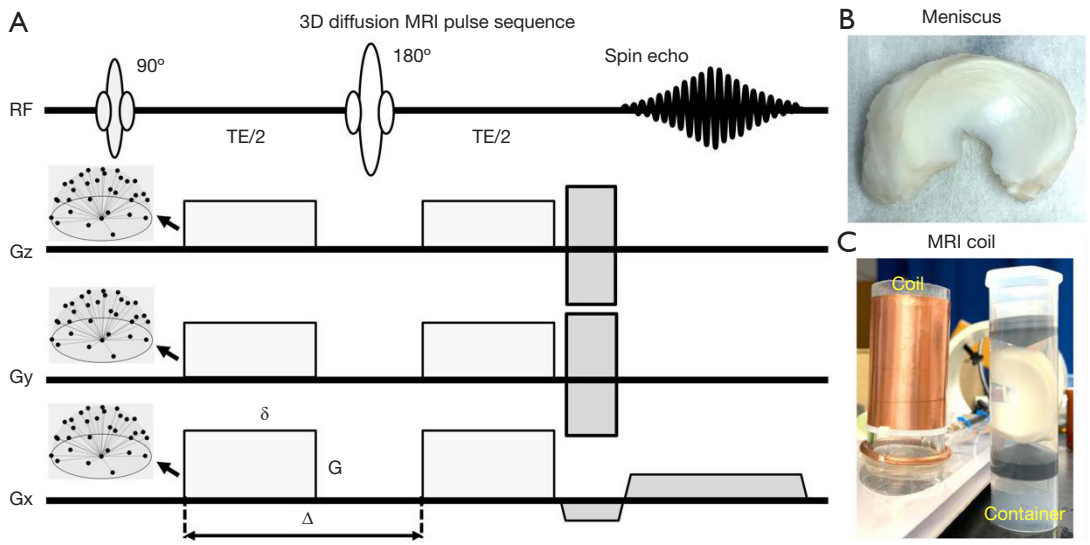

Figure 1 A 3D diffusion-weighted spin-echo pulse sequence with the diffusion-encoding directions (black arrows) (A) was employed to image the meniscus (B) using a specimen container and custom-made RF coil (C). TE is the echo time, G is the strength of the gradient pulse, δ is the duration of the pulse, and Δ is the time between pulses. 3D, three-dimensional; MRI, magnetic resonance imaging; RF, radio frequency.

The scan time was about 4.5 hours for each b value. The diffusion gradient orientations were optimized to ensure the uniformity of the encoding directions. The gradient separation time was 5.5 ms and the diffusion gradient duration time was 4.7 ms for all scans. The maximum gradient amplitude was about 56 G/cm. The temperature was monitored throughout all scans and the fluctuations were less than 1 ℃. Following MR imaging, menisci were processed for histological analysis as described below.

Tractography and track density imaging (TDI)

All diffusion-weighted images (DWIs) were registered to the baseline b0 images using the affine transformation model in Advanced Normalization Tools (ANTs) (28). Two different diffusion MRI models were used to analyze the data. First, the DTI model was used to characterize the primary fiber direction in the meniscus (24,29). Next, generalized q-sampling imaging (GQI) was used to quantify the water diffusion properties at different orientations. Deterministic fiber tracking was performed for the whole meniscus (30). The tracking was repeated until the tracking trajectory exceeded the turning angle by more than 45°. A threshold of 0.05 was set for both fractional anisotropy and quantitative anisotropy with the maximum streamline length of 200 mm. TDI was also used to visualize the microstructure of the whole meniscus after tractography was generated (30). The total number of tracks present in each element of the grid was then calculated. Super-resolution TDI maps were generated at grid sizes of 500, 250, 125, and 62.5 μm. Because the grid element can be smaller than the acquired voxel size, the resolution of the final map can be higher than that of the original dMRI data (31). All fiber tracking operations were performed using DSI studio toolbox (30).

Histology

Menisci were sliced radially (perpendicular to the tibial plateau) to allow cross-sectional analysis. Tissue samples were then dehydrated, embedded in paraffin, and sectioned at 8 μm. The sections were stained with Safranin-O (Sigma-Aldrich, St. Louis, MO, USA), 0.02% aqueous fast green (Electron Microscopy Sciences, Hatfield, PA, USA), and Harris hematoxylin (Electron Microscopy Sciences) (32-35). The stained sections were imaged using a brightfield Olympus BX53F microscope.

Results

Distinct differences were observed in the fiber orientation images derived from DTI and GQI. Specifically, DTI only

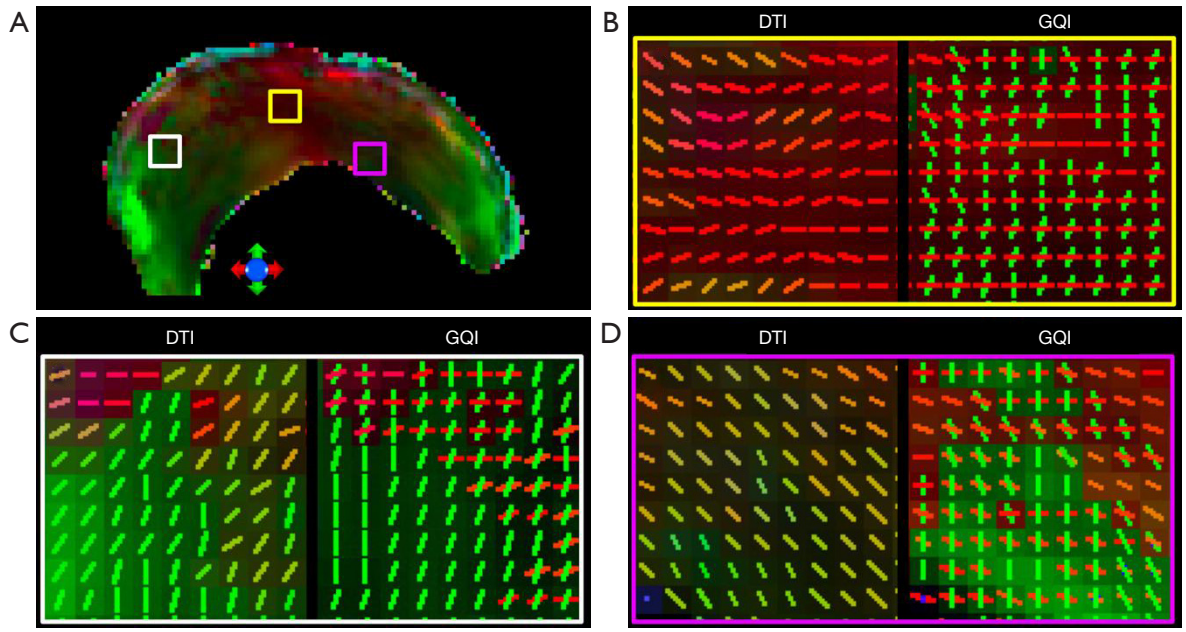

Figure 2 There are numerous crossing fibers evident in each voxel of the meniscus using GQI and only a single fiber direction in each voxel using DTI. The colors represent different fiber orientations, with red denoting a horizontal fiber orientation, green denoting a vertical fiber orientation, and blue denoting a fiber orientation perpendicular to red and green. Results are depicted with a b value of 1,000 s/mm^2. DTI, diffusion tensor imaging; GQI, generalized q-sampling imaging.

provided a single fiber orientation in each voxel (*Figure 2*). In contrast, using GQI, both circumferential fibers and radial fibers could be detected.

Differences in tractography were also observed between DTI and GQI (*Figure 3*). Using GQI reconstruction, numerous crossing fibers were resolved in the meniscus. However, DTI failed to accurately quantify the 3D fiber architecture in regions where crossing fibers were observed with GQI.

Furthermore, using GQI, better organized tracts were observed at a b value of 1000 s/mm^2 compared to a b-value of 100 s/mm^2 (*Figure 4*). Tractography of the whole meniscus is also presented in Video S1.

Importantly, the fiber orientations measured from GQI were consistent with fiber orientations observed from Safranin O/Fast Green stained histological sections (*Figure 5*). Fiber orientations varied with location throughout the meniscus. The central region of the meniscus towards the femoral side was dominated by circumferential fibers, as well as some radial fibers, and on histological sections the matrix alignment appeared similar. The surface of the meniscus adjacent to the tibia was primarily composed of collagen fibers parallel to the tissue surface, with some circumferential fibers.

Finally, it was possible to derive high resolution tract density images with GQI reconstructions (*Figure 6*). Both circumferential and radial fibrils were resolved from TDI. Not surprisingly, the complex fiber structures were better resolved at higher spatial resolution.

Discussion

In this study, we successfully used dMRI to probe the microstructure of porcine menisci using a HARDI acquisition with both DTI and GQI reconstruction methods. Importantly, we were able to resolve both radial and circumferential collagen fibers with GQI reconstruction in different regions throughout the meniscus. In contrast, for DTI, only a single fiber orientation was observed in each voxel. These findings demonstrate the advantage of GQI over DTI to visualize the complex collagen fiber orientation in menisci.

Previous assessments of meniscal architecture have used techniques such as scanning electron microscopy, polarized light microscopy, and reflectance confocal microscopy to quantify the collagen fiber organization throughout the meniscal tissue (2,36,37). These previous studies have documented the presence of radial and circumferential

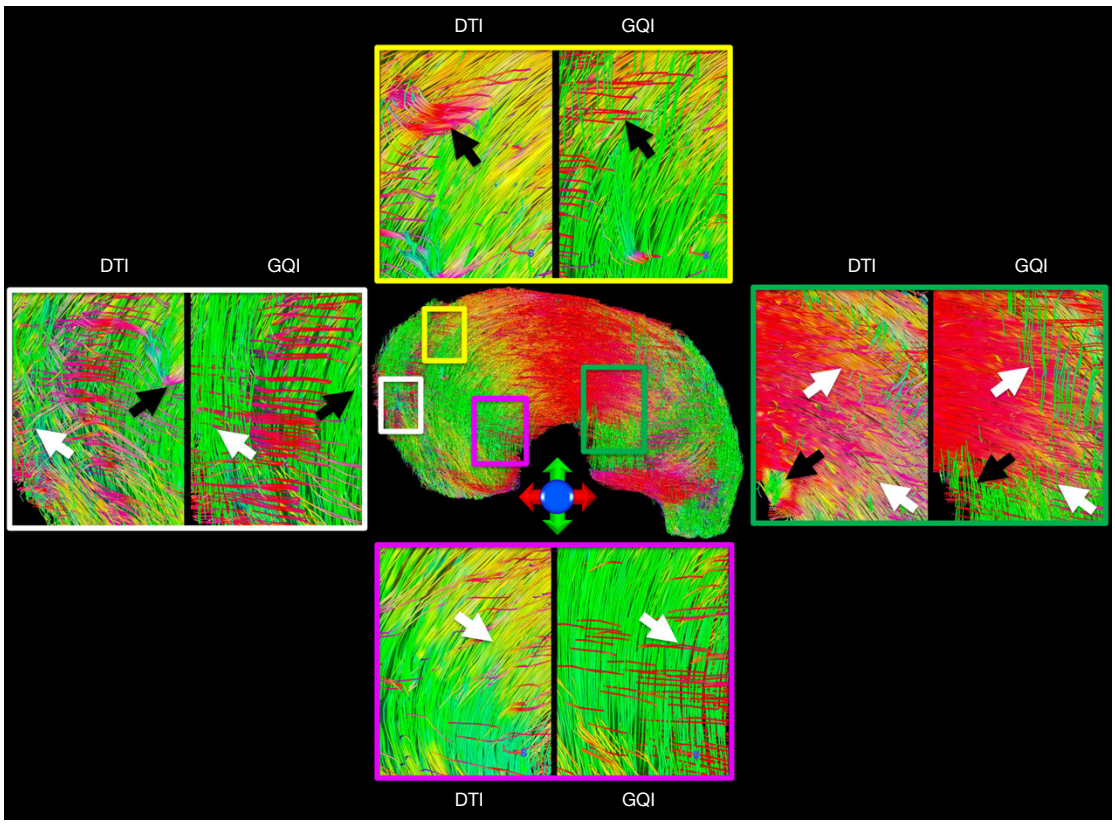

Figure 3 Tractography images were derived from DTI and GQI throughout the meniscus. Numerous crossing fibers were resolved in the meniscus using GQI (white arrows). DTI failed to accurately quantify the 3D fiber architecture in regions where crossing fibers were observed with GQI (black arrows). The colors represent different fiber orientations, with red denoting a horizontal fiber orientation, green denoting a vertical fiber orientation, and blue denoting a fiber orientation perpendicular to red and green. Results are depicted with a b value of 1,000 s/mm^2. DTI, diffusion tensor imaging; GQI, generalized q-sampling imaging; 3D, three-dimensional.

fibers that vary with location within the meniscus. Although these methods provide much higher spatial resolution than MRI, the images often only capture a small region of the meniscus in 2D and can suffer from geometric distortions introduced by sectioning (36,37). In contrast, MRI offers a non-invasive means to investigate 3D tissue organization.

Multiple MRI techniques have been used to characterize meniscal structure. T2 values decreased steadily from the outer to the inner zone of the meniscus (38). Furthermore, T2 and T2* relaxation times have been used to estimate the collagen fiber alignment in the meniscus (12,39,40). However, in order to accurately estimate the collagen fiber alignment in 3D, these measurements require separate scans at different orientations with respect to the main magnetic field (39). Alternatively, dMRI provides a straightforward method to quantify the meniscus diffusivity properties and to visualize the 3D fiber alignment (22). The diffusion signal decay can be detected at different gradient encoding directions, which do not require physical rotation of the specimen. Unfortunately, multiple orientations of fibers within a voxel are poorly detected using DTI. However, our results demonstrate that tractography using GQI and super-resolution TDI have the ability to probe the 3D fiber architecture at the intravoxel level. Notably, only one major fiber orientation was detected in each voxel using DTI, whereas using GQI allowed for multiple fiber directions to be detected in different regions of the meniscus.

Prior work has demonstrated higher diffusivity values in the inner zone of the meniscus (23), which may be related to the less restricted water molecules in this region due to higher concentrations of negatively charged proteoglycans (41). Additionally, prior work has shown that there is a higher fractional anisotropy in the outer zone, which may be related to the dense fibular network (23).

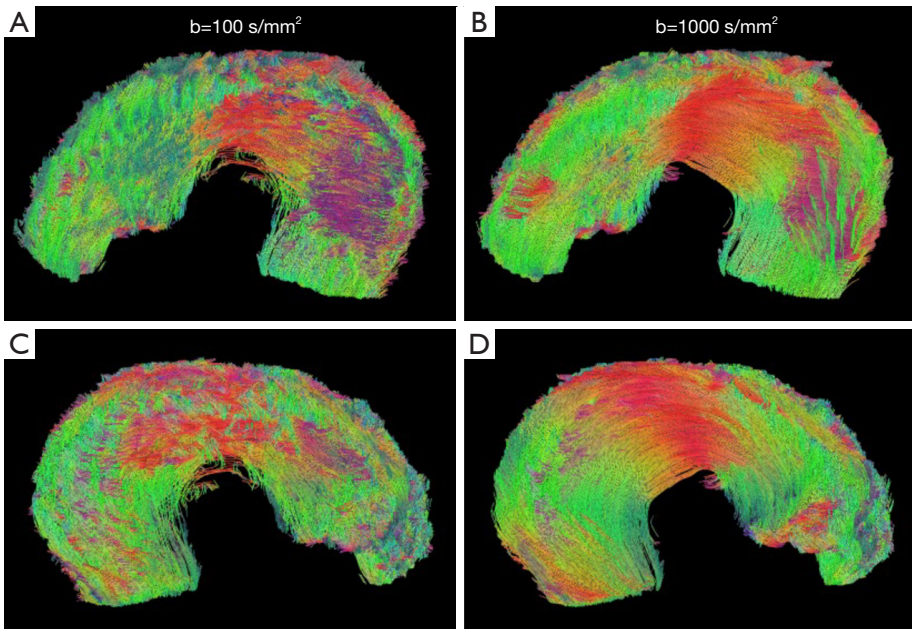

Figure 4 Tractography results of the meniscus were generated using GQI reconstruction at different diffusion gradients (100 and 1,000 s/mm^2). (A,B) are superior views and (C,D) are inferior views. The tractography is visually comparable at the two different b values, with better organized tracts at the higher b value. GQI, generalized q-sampling imaging.

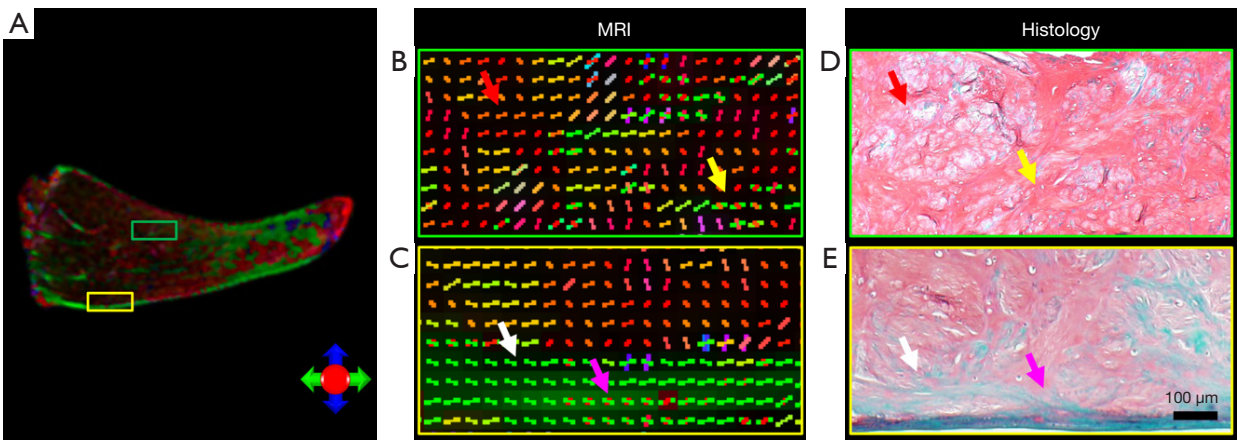

Figure 5 Fiber orientation images of meniscus were generated using GQI (A,B,C), with corresponding Safranin O (red = proteoglycans)/ fast green (blue = collagen) stained histology (D,E). The green box is near the femoral surface and the yellow box is adjacent to the tibial surface. The matrix orientation in histology is similar to the MRI findings (red, yellow, white, and purple arrows). The colors (panels A,B,C) represent different fiber orientations, with green denoting a horizontal fiber orientation, blue denoting a vertical fiber orientation, and red denoting a fiber orientation perpendicular to green and blue. GQI, generalized q-sampling imaging; MRI, magnetic resonance imaging.

These differences in meniscus structure with location are consistent with the inhomogeneous tractography measurements in the current study. Importantly, these tractography results were consistent with histological assessments.

Meniscal damage is a risk factor for the development of OA (3). Loss of meniscus integrity predisposes the adjacent articular cartilage to increased axial and shear stresses, which may result in cartilage degeneration (42,43). Recently, Seitz *et al.* demonstrated that OA-related degeneration alters

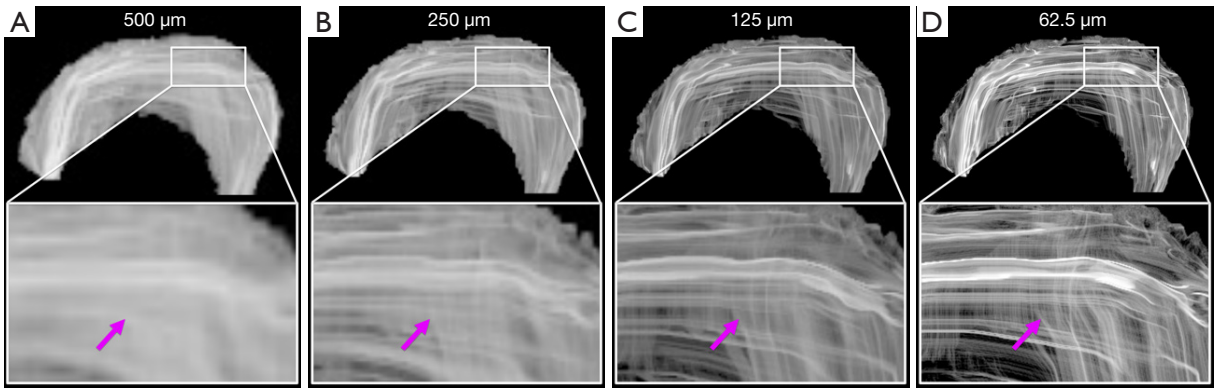

Figure 6 Representative TDI generated from GQI reconstruction at different spatial resolutions in 2D (A-D), ranging from 500 to 62.5 μm. The complex fiber structures (including the presence of crossing fibers) are better resolved with higher spatial resolution TDI (purple arrows). TDI, track density imaging; GQI, generalized q-sampling imaging; 2D, two-dimensional.

the biomechanical properties of human menisci before the articular cartilage (44). However, these mechanical property measurements can currently only be performed on *ex vivo* tissues. The capability to measure multiple fiber directions within each voxel with HARDI acquisition and GQI reconstruction could potentially be utilized *in vivo* to identify early-stage disruption of the 3D architecture of the meniscus, which may lead to subsequent meniscal tears, joint degeneration, and the development of OA.

This study is not without limitations. Scans were performed on a preclinical magnet with a high diffusion gradient coil and high magnetic field. While the scan time was very long for the current study, it could be reduced with lower spatial resolution, angular resolution, and novel acquisition methods. Furthermore, a contrast agent was utilized to improve the signal to noise ratio. Thus, translating these techniques to clinical scanners will likely require both novel acquisition and reconstruction techniques (45). Despite these hurdles, the use of these imaging techniques to investigate early changes in meniscal tissue structure and organization warrants further investigation.

In summary, using HARDI acquisition with GQI reconstruction, we could resolve crossing fibers in the meniscus. On the other hand, only a single fiber orientation was measured within each voxel using the conventional DTI method. Therefore, GQI reconstruction is able to better assess the complex 3D structure of the meniscus. In the future, these technologies may have the potential to nondestructively assess both normal and abnormal meniscal structure in the clinical environment.

Acknowledgments

The authors thank Dr. G. Allan Johnson (Duke University, NIH/NIBIB P41 EB015897) for access to the MRI scanner. The authors also thank James Cook (Duke University), Dawn Chasse (Duke University), and Lucy Upchurch (Duke University) for significant technical support.

Funding: This work was supported by NIH grants (Nos. AR073221, AR079184, AR078245, AR074800, and AR065527), the Strategic Research Initiative (SRI) at Indiana University Health and Indiana University School of Medicine, and the Charles E. Putman MD Vision Award from the Department of Radiology at Duke University School of Medicine.

Footnote

Conflicts of Interest: All authors have completed the ICMJE uniform disclosure form (available at https://qims.amegroups.com/article/view/10.21037/qims-23-1355/coif). A.L.M. reports receiving NIH support through grants (Nos. AR073221, AR079184, AR078245). The other authors have no conflicts of interest to declare.

Ethical Statement: The authors are accountable for all aspects of the work in ensuring that questions related to the accuracy or integrity of any part of the work are appropriately investigated and resolved.

References

1. Eyre DR, Wu JJ. Collagen of fibrocartilage: a distinctive molecular phenotype in bovine meniscus. FEBS Lett 1983;158:265-70.
2. Li Q, Qu F, Han B, Wang C, Li H, Mauck RL, Han L. Micromechanical anisotropy and heterogeneity of the meniscus extracellular matrix. Acta Biomater 2017;54:356-66.
3. Englund M, Guermazi A, Roemer FW, Aliabadi P, Yang M, Lewis CE, Torner J, Nevitt MC, Sack B, Felson DT. Meniscal tear in knees without surgery and the development of radiographic osteoarthritis among middle-aged and elderly persons: The Multicenter Osteoarthritis Study. Arthritis Rheum 2009;60:831-9.
4. De Filippo M, Bertellini A, Pogliacomi F, Sverzellati N, Corradi D, Garlaschi G, Zompatori M. Multidetector computed tomography arthrography of the knee: diagnostic accuracy and indications. Eur J Radiol 2009;70:342-51.
5. De Smet AA. How I diagnose meniscal tears on knee MRI. AJR Am J Roentgenol 2012;199:481-99.
6. Nguyen JC, De Smet AA, Graf BK, Rosas HG. MR imaging-based diagnosis and classification of meniscal tears. Radiographics 2014;34:981-99.
7. Terzidis IP, Christodoulou A, Ploumis A, Givissis P, Natsis K, Koimtzis M. Meniscal tear characteristics in young athletes with a stable knee: arthroscopic evaluation. Am J Sports Med 2006;34:1170-5.
8. Lefevre N, Naouri JF, Herman S, Gerometta A, Klouche S, Bohu Y. A Current Review of the Meniscus Imaging: Proposition of a Useful Tool for Its Radiologic Analysis. Radiol Res Pract 2016;2016:8329296.
9. Anz AW, Lucas EP, Fitzcharles EK, Surowiec RK, Millett PJ, Ho CP. MRI T2 mapping of the asymptomatic supraspinatus tendon by age and imaging plane using clinically relevant subregions. Eur J Radiol 2014;83:801-5.
10. Bolog NV, Andreisek G. Reporting knee meniscal tears: technical aspects, typical pitfalls and how to avoid them. Insights Imaging 2016;7:385-98.
11. Filho GH, Du J, Pak BC, Statum S, Znamorowski R, Haghighi P, Bydder G, Chung CB. Quantitative characterization of the Achilles tendon in cadaveric specimens: T1 and T2* measurements using ultrashort-TE MRI at 3 T. AJR Am J Roentgenol 2009;192:W117-24.
12. Wang N, Xia Y. Orientational dependent sensitivities of T2 and T1ρ towards trypsin degradation and Gd-DTPA2- presence in bovine nasal cartilage. MAGMA 2012;25:297-304.
13. Bolbos RI, Link TM, Ma CB, Majumdar S, Li X. T1rho relaxation time of the meniscus and its relationship with T1rho of adjacent cartilage in knees with acute ACL injuries at 3 T. Osteoarthritis Cartilage 2009;17:12-8.
14. Juras V, Apprich S, Zbýň Š, Zak L, Deligianni X, Szomolanyi P, Bieri O, Trattnig S. Quantitative MRI analysis of menisci using biexponential T2* fitting with a variable echo time sequence. Magn Reson Med 2014;71:1015-23.
15. Krishnan N, Shetty SK, Williams A, Mikulis B, McKenzie C, Burstein D. Delayed gadolinium-enhanced magnetic resonance imaging of the meniscus: an index of meniscal tissue degeneration? Arthritis Rheum 2007;56:1507-11.
16. Rauscher I, Stahl R, Cheng J, Li X, Huber MB, Luke A, Majumdar S, Link TM. Meniscal measurements of T1rho and T2 at MR imaging in healthy subjects and patients with osteoarthritis. Radiology 2008;249:591-600.
17. Stehling C, Luke A, Stahl R, Baum T, Joseph G, Pan J, Link TM. Meniscal T1rho and T2 measured with 3.0T MRI increases directly after running a marathon. Skeletal Radiol 2011;40:725-35.
18. Baboli R, Sharafi A, Chang G, Regatte RR. Biexponential T(1ρ) relaxation mapping of human knee menisci. J Magn Reson Imaging 2019;50:824-35.
19. Williams A, Qian Y, Golla S, Chu CR. UTE-T2* mapping detects sub-clinical meniscus injury after anterior cruciate ligament tear. Osteoarthritis Cartilage 2012;20:486-94.
20. Du J, Carl M, Diaz E, Takahashi A, Han E, Szeverenyi NM, Chung CB, Bydder GM. Ultrashort TE T1rho (UTE T1rho) imaging of the Achilles tendon and meniscus. Magn Reson Med 2010;64:834-42.
21. Wang N, Mirando AJ, Cofer G, Qi Y, Hilton MJ, Johnson GA. Diffusion tractography of the rat knee at microscopic resolution. Magn Reson Med 2019;81:3775-86.
22. Jeurissen B, Descoteaux M, Mori S, Leemans A. Diffusion MRI fiber tractography of the brain. NMR Biomed 2019;32:e3785.

23. Shen J, Zhao Q, Qi Y, Cofer G, Johnson GA, Wang N. Tractography of Porcine Meniscus Microstructure Using High-Resolution Diffusion Magnetic Resonance Imaging. Front Endocrinol (Lausanne) 2022;13:876784.
24. Basser PJ, Mattiello J, LeBihan D. MR diffusion tensor spectroscopy and imaging. Biophys J 1994;66:259-67.
25. Wang N, Mirando AJ, Cofer G, Qi Y, Hilton MJ, Johnson GA. Characterization complex collagen fiber architecture in knee joint using high-resolution diffusion imaging. Magn Reson Med 2020;84:908-19.
26. Tuch DS. Q-ball imaging. Magn Reson Med 2004;52:1358-72.
27. Yeh FC, Tseng WY. NTU-90: a high angular resolution brain atlas constructed by q-space diffeomorphic reconstruction. Neuroimage 2011;58:91-9.
28. Avants BB, Tustison NJ, Song G, Cook PA, Klein A, Gee JC. A reproducible evaluation of ANTs similarity metric performance in brain image registration. Neuroimage 2011;54:2033-44.
29. Yeh FC, Wedeen VJ, Tseng WY. Generalized q-sampling imaging. IEEE Trans Med Imaging 2010;29:1626-35.
30. Yeh FC, Verstynen TD, Wang Y, Fernández-Miranda JC, Tseng WY. Deterministic diffusion fiber tracking improved by quantitative anisotropy. 2013;8:e80713.
31. Calamante F, Tournier JD, Jackson GD, Connelly A. Track-density imaging (TDI): super-resolution white matter imaging using whole-brain track-density mapping. Neuroimage 2010;53:1233-43.
32. McNulty AL, Moutos FT, Weinberg JB, Guilak F. Enhanced integrative repair of the porcine meniscus in vitro by inhibition of interleukin-1 or tumor necrosis factor alpha. Arthritis Rheum 2007;56:3033-42.
33. McNulty AL, Weinberg JB, Guilak F. Inhibition of matrix metalloproteinases enhances in vitro repair of the meniscus. Clin Orthop Relat Res 2009;467:1557-67.
34. Riera KM, Rothfusz NE, Wilusz RE, Weinberg JB, Guilak F, McNulty AL. Interleukin-1, tumor necrosis factor-alpha, and transforming growth factor-beta 1 and integrative meniscal repair: influences on meniscal cell proliferation and migration. Arthritis Res Ther 2011;13:R187.
35. Wilusz RE, Weinberg JB, Guilak F, McNulty AL. Inhibition of integrative repair of the meniscus following acute exposure to interleukin-1 in vitro. J Orthop Res 2008;26:504-12.
36. Campo-Ruiz V, Patel D, Anderson RR, Delgado-Baeza E, González S. Evaluation of human knee meniscus biopsies with near-infrared, reflectance confocal microscopy. A pilot study. Int J Exp Pathol 2005;86:297-307.
37. Petersen W, Tillmann B. Collagenous fibril texture of the human knee joint menisci. Anat Embryol (Berl) 1998;197:317-24.
38. Chiang SW, Tsai PH, Chang YC, Wang CY, Chung HW, Lee HS, Chou MC, Hsu YC, Huang GS. T2 values of posterior horns of knee menisci in asymptomatic subjects. PLoS One 2013;8:e59769.
39. Hager B, Walzer SM, Deligianni X, Bieri O, Berg A, Schreiner MM, Zalaudek M, Windhager R, Trattnig S, Juras V. Orientation dependence and decay characteristics of T(2) * relaxation in the human meniscus studied with 7 Tesla MR microscopy and compared to histology. Magn Reson Med 2019;81:921-33.
40. Wang N, Kahn D, Badar F, Xia Y. Molecular origin of a loading-induced black layer in the deep region of articular cartilage at the magic angle. J Magn Reson Imaging 2015;41:1281-90.
41. Sanchez-Adams J, Willard VP, Athanasiou KA. Regional variation in the mechanical role of knee meniscus glycosaminoglycans. J Appl Physiol (1985) 2011;111:1590-6.
42. Carter TE, Taylor KA, Spritzer CE, Utturkar GM, Taylor DC, Moorman CT 3rd, Garrett WE, Guilak F, McNulty AL, DeFrate LE. In vivo cartilage strain increases following medial meniscal tear and correlates with synovial fluid matrix metalloproteinase activity. J Biomech 2015;48:1461-8.
43. Englund M, Guermazi A, Lohmander SL. The role of the meniscus in knee osteoarthritis: a cause or consequence? Radiol Clin North Am 2009;47:703-12.
44. Seitz AM, Osthaus F, Schwer J, Warnecke D, Faschingbauer M, Sgroi M, Ignatius A, Dürselen L. Osteoarthritis-Related Degeneration Alters the Biomechanical Properties of Human Menisci Before the Articular Cartilage. Front Bioeng Biotechnol 2021;9:659989.
45. Wengler K, Tank D, Fukuda T, Paci JM, Huang M, Schweitzer ME, He X. Diffusion tensor imaging of human Achilles tendon by stimulated echo readout-segmented EPI (ste-RS-EPI). Magn Reson Med 2018;80:2464-74.

Cite this article as: Zhao Q, Holt A, Spritzer CE, DeFrate LE, McNulty AL, Wang N. High angular resolution diffusion imaging (HARDI) of porcine menisci: a comparison of diffusion tensor imaging and generalized q-sampling imaging. Quant Imaging Med Surg 2024;14(4):2738-2746. doi: 10.21037/qims-23-1355

